The Interpretation of Comparative Half-Lives in the Fermi Theory of Beta-Decay*

EUGENE FEENBERG AND GEORGE TRIGG

Washington University, St. Louis, Missouri

THE ft product, or comparative half-life, in the Fermi theory of beta-decay provides a useful criterion for the classification of radioactive transitions as allowed or forbidden to various degrees.[1] Here f is a theoretical factor which corrects the observed half-life t for the effects of the nuclear charge and the energy of the transition, thus reducing all half-lives to a comparable basis. Appendix A contains the general formulas for f and a description of procedures for calculating. Figures 1–9 are charts of f values as functions of Z and W_0.

The relation

$$ft=2\pi^3(2I_i+1)\ \ln 2/G^2\cdot\Sigma|(f|M|i)|^2 \qquad (1)$$

connects the ft product with the Fermi constant G, the nuclear matrix element $(f/M/i)$ of the β-transition and the spin I_i of the parent nucleus. The factor $(2I_i+1)^{-1}$ is the statistical weight of a single magnetic substate of the parent nucleus. A sum over all combinations of initial and final magnetic quantum numbers is indicated by the summation symbol.

Image transitions, for which $ft<10^4$, are particularly interesting and have been studied by several authors;[2–4] the empasis in the present discussion is on the range $ft>10^4$ comprising the allowed unfavored type of transition and all forbidden types.

The authors have prepared tables of revelant information (as of November, 1949) on all transitions for which the determinations of energy, half-life and branching ratios appear to be sufficiently accurate and complete to permit the calculation of the ft product.** This information may be faulty in detail, but should be adequate, or nearly so, for statistical analysis of the type embodied in Figs. 10 and 11.

All positron transitions are corrected for K-capture, whether observed or not, by using for f the sum of f_+ and f_k (Figs. 6–7). Transitions between ground states from even-even to odd-odd require a correction factor $2I_f+1$ multiplying ft to make a quantity comparable with the ft values of odd-odd to even-even transitions.[5]

Transitions for which $\log(W_0^2-1)ft\sim10$ include Cl^{38}, A^{41}, K^{42}, Sr^{89}, Sr^{90}, Y^{90}, Y^{91}, and Cs^{137}. There is good evidence that most of these are first forbidden[6–8] with $\Delta I=\pm2$. The factor W_0^2-1 is approximately proportional to the average value of the function $W^2-1+(W-W_0)^2$ over the allowed energy distribution.

Figures 10 and 11 are histograms[9] showing the distribution of $\log ft$ values. The transitions listed in the preceding paragraph are excluded. Separate curves are provided for (a) odd A, transitions between ground states, (b) all transitions for odd A, all transitions involving an excited state of the even-even nucleus for even A, (c) even A, all transitions between ground states.

This classification is motivated by the empirical rule that even-even nuclei have zero spin in the ground state. Thus in Fig. 11 one of the two states involved in a transition has zero spin and presumably even parity.

Consider first Fig. 10. The image transitions extending from $n_0^1\rightarrow H_1^1$ to $Ti_{21}^{41}\rightarrow Ca_{20}^{41}$ make up the allowed favored group centered at $\log ft\sim3.55$. A blank region between 3.95 and 4.55 is followed by the allowed unfavored group with two peaks at 5.00 and 5.50. The appearance of two peaks in this region may be illusory, the result of a large statistical fluctuation. For the moment it seems necessary to state the apparent fact without attempting an interpretation.

Continuing to the right the next group has a peak near $\lg ft\sim6.2$. Included are Ni^{65}(6.6), Ga^{73}(5.9), As^{77}(6.0), Zr^{89}(6.3), Pd^{101}(6.4), Pd^{109}(6.1), Cd^{117}(6.1), Ag^{115}(6.4), In^{115}(6.4), In^{117}(6.4), In^{119}(6.2), Xe^{137}(6.3), Nd^{149}(6.2), Er^{169}(6.1), Y^{177}(6.20), Pt^{197}(6.2), and Pt^{199}(6.25) and Ra^{225}(6.1) for transitions to the ground state of the product nucleus. This group is identified as predominantly first forbidden[10] since all possibilities for

* Partially assisted by the joint program of the ONR and the AEC.

[1] E. J. Konopinski and G. E. Uhlenbeck, Phys. Rev. **60**, 308 (1941); E. J. Konopinski, Rev. Mod. Phys. **15**, 209 (1943). Familiarity with the ideas and terminology of these references is assumed.

[2] B. O. Grönblom, Phys. Rev. **56**, 508 (1939).

[3] E. P. Wigner, Phys. Rev. **56**, 519 (1939).

[4] A. M. Feingold and E. P. Wigner [unpublished notes (1949)].

** *Note added in proof:* the following paper by A. M. Feingold presents a similar more complete table including data from recent publications (through June, 1950).

[5] R. E. Marshak, Phys. Rev. **61**, 431 (1942), particularly p. 433 and reference 18.

[6] E. Feenberg and K. C. Hammack, Phys. Rev. **75**, 1877 (1949).

[7] F. B. Shull and E. Feenberg, Phys. Rev. **75**, 1768 (1949).

[8] N. Feather and H. O. W. Richardson, Proc. Phys. Soc. London **61**, 452 (1948).

[9] In constructing the histograms the abscissa is first divided into intervals of length 0.125 beginning at 3.000. The total number of examples in each pair of adjacent intervals is plotted as an ordinate extending over a range 0.125 symmetrically placed with respect to the two intervals. Each transition contributes to two adjacent ordinates, resulting in considerable smoothing of statistical fluctuations.

[10] It is true that allowed unfavored transitions with exceptionally small nuclear matrix elements cannot be excluded on theoretical grounds. Possibly a number of transitions with $\lg ft>6$ are really of the allowed type.

allowed transitions are exhausted by the favored and unfavored classifications. A well-defined group requires a nuclear matrix element relatively independent of Z and W_0; the matrix elements of α in the tensor coupling theory and of γ_5 in the axial vector theory are suitable in this respect and are also larger, on the average, than other first forbidden matrix elements.

Beyond the first forbidden peak the ordinate descends in an irregular manner giving no indication of a clean cut separation of different types of first forbidden and second forbidden transitions.

No distinction has been drawn between the solid and dashed curves of Fig. 10. The close similarity means that transitions to excited states for both even and odd A are not significantly different as regards the distribution of comparitive half-lives from those to the ground states of odd nuclei.

Turning now to Fig. 11 the first group on the left contains three examples: $He_2^6 \rightarrow Li_2^6$, $F_9^{18} \rightarrow O_8^{18}$ and $Al_{13}^{26} \rightarrow Mg_{12}^{26}$. These may all be interpreted as transitions between $^1S_0$ and $^3S_1$ ground states with nearly identical space wave functions in accordance with Wigner's theory of nuclear supermultiplets.[3]

The next group centered at $\log ft(2I_f+1) \sim 4.4$ includes B_5^{12}, N_7^{12}, Pd_{46}^{112}, In_{49}^{112} (both β^+ and β^-), In_{49}^{114}, In_{49}^{116}, Sb_{51}^{118}, and Sb_{51}^{120}. The first two are perhaps in a special category because of their extremely large transition energies, although it is not clear how this fact helps account for the small value of ft. From the narrow range of Z and A covered by the others it is reasonable to conclude that the nuclear property involved is not a random statistical feature of nuclear structure. With six examples at $Z=49$ and 51 an explanation of the small ft values may be sought in the properties of the proton shell which closes at $Z=50$.

What is needed is an exceptionally large admixture of components belonging to higher supermultiplets in the ground state wave function of the nucleus with the smaller value of $|N-Z|$. This effect may be correlated with the extreme nonuniform particle density predicted

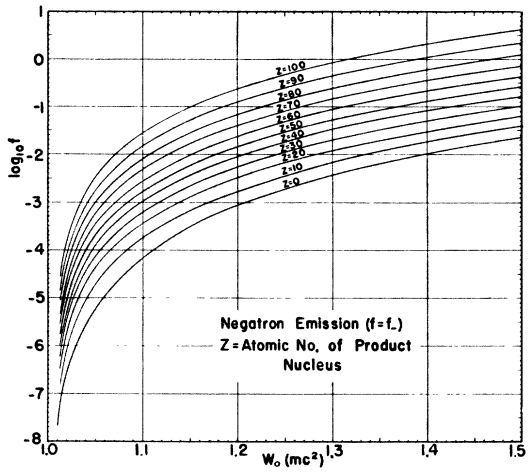

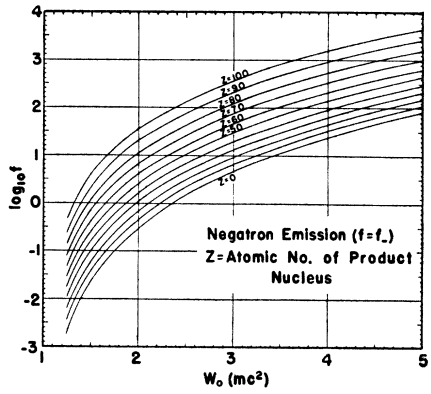

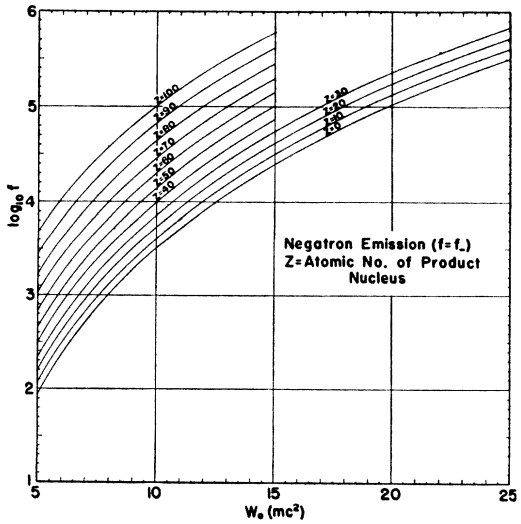

FIGS. 1–3. The function $f(Z, W_0)$ for negatron emission.

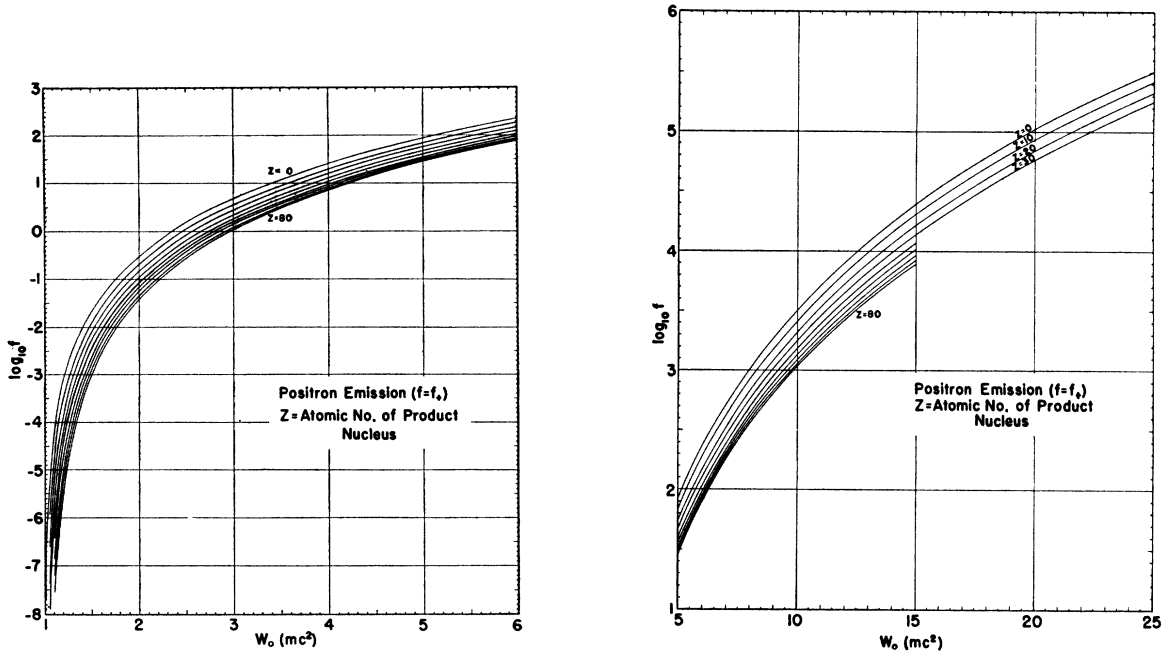

FIGS. 4–5. The function $f(Z, W_0)$ for positron emission alone; to be used in conjunction with the partial half-life for positron emission. These curves are useful when the K-capture to positron ratio is known.

by the central elevation shell model in a small range[11] including $Z=50$.

A broad group centered at $\log ft(2I_f+1)\sim 5.1$ is interpreted as allowed, but unfavored to the same extent as corresponding transitions in odd nuclei.

Next comes the outstanding feature of the histogram for even A, the complete absence of a group on the range 5.7–6.7 corresponding to the well-defined first forbidden peak centered at $\log ft\sim 6.2$. Both tensor and axial vector coupling theories permit unforced interpre-

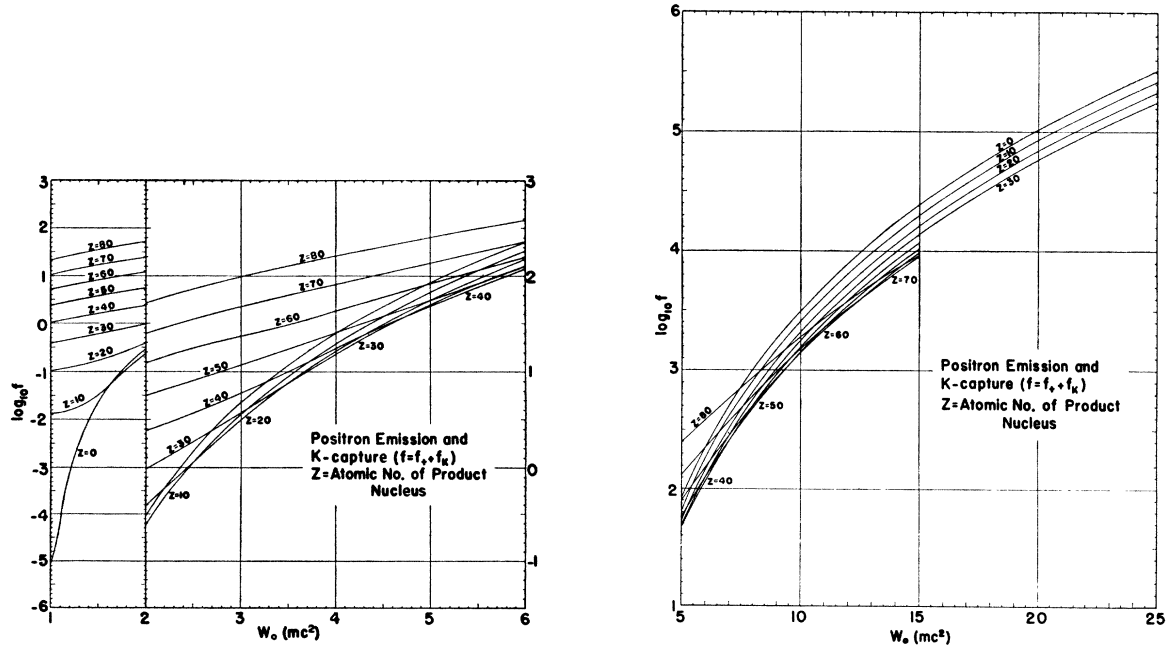

FIGS. 6–7. The function $f(Z, W_0)$ for positron emission and K-capture; to be used in conjunction with the experimental half-life whether or not K-capture has been observed. The correction for capture is included in f.

[11] Bounded below by the $2s$, $2p$: lg crossovers near $Z=47$ and above by the uniformizing tendency of the occupied $2d$ orbits. Most of the odd neutron nuclei with $I=\frac{1}{2}$ occur in this range.

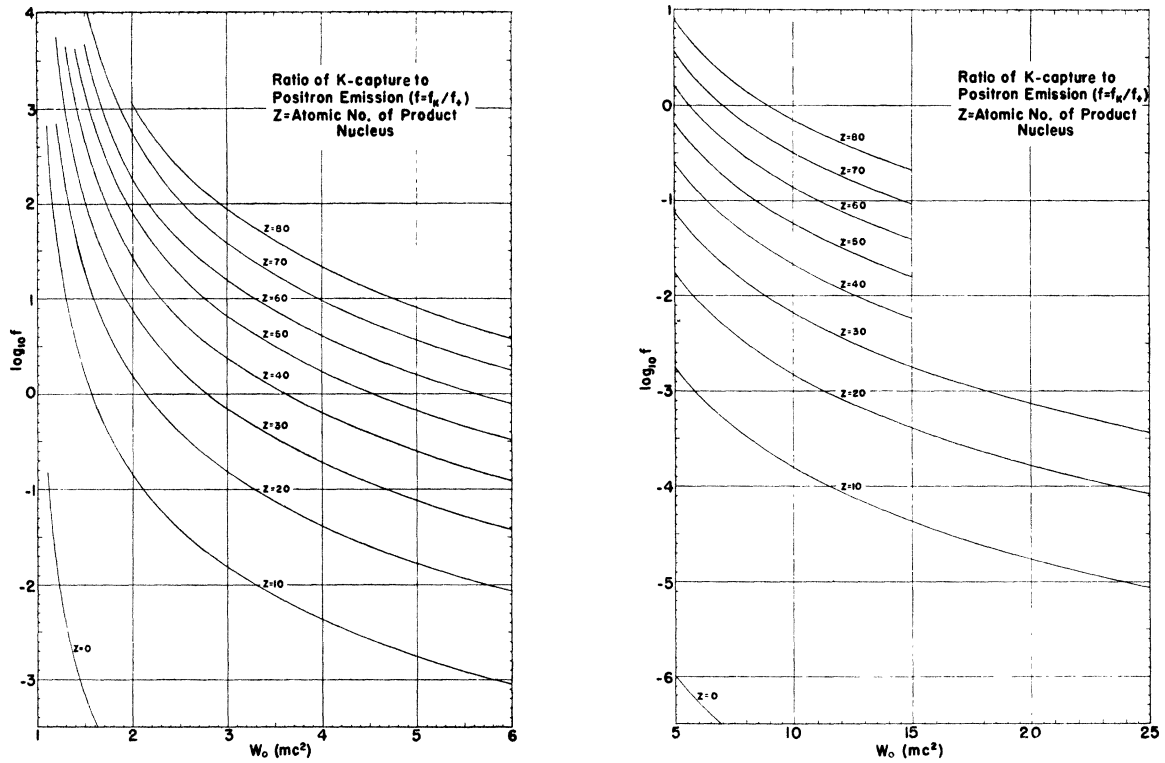

FIGS. 8–9. The function $f_K(Z, W_0)/f_+(Z, W_0)$. For allowed transitions this function gives the theoretical K-capture to positron ratio.

tations of the "missing" group in terms of the properties of the α- and γ_5-matrix elements. A discussion of the theory follows.

TENSOR COUPLING

In the non-relativistic approximation $\boldsymbol{\alpha}$ reduces to $\mathbf{p}/Mc$ where $\mathbf{p}$ is the linear momentum operator of a nucleon.[12] To account for the "missing" group it is necessary that the matrix elements of $\boldsymbol{\alpha}$ between ground states for even A should be considerably smaller than the corresponding quantities for odd A. The following hypotheses are sufficient for this purpose: (a) $I=0$ for ground states of even-even nuclei; (b) These states are even and predominantly of the $^1S_0$ type; (c) Odd-odd nuclei with odd parity and $I=1$ in the ground state are predominantly of the triplet type ($^3S_1+^3P_1+^3D_1$).

Hypothesis a requires no argument; b and c yield the desired conclusion since the linear momentum operators do not connect singlet and triplet states. Incidently b and c are at an opposite extreme from the hypothesis of extreme spin-orbit coupling ($j-j$ coupling shell model).[13,14]

AXIAL VECTOR COUPLING

In the non-relativistic approximation γ_5 reduces to $\boldsymbol{\sigma}\cdot\mathbf{p}/Mc$ where $\boldsymbol{\sigma}$ and $\mathbf{p}$ are spin operators and linear

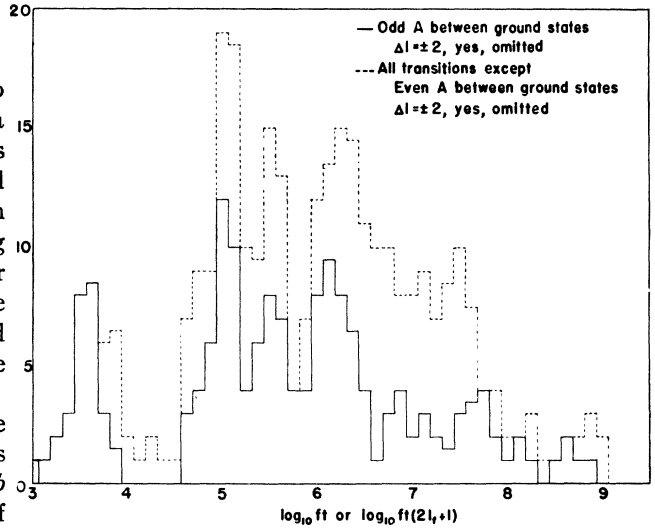

FIG. 10. Histograms of ft values. The solid line represents transitions between ground states of odd nuclei; the dotted line, all transitions except those between ground states of even nuclei. Transitions involving a spin change of two units and a parity change are omitted. The abscissa is $\log_{10} ft(2I_f+1)$ for transitions in which the parent nucleus is even-even, and $\log_{10} ft$ for all others.

[12] E. L. Hill and R. Landshoff, Rev. Mod. Phys. **10**, 87 (1938).
[13] Haxel, Jensen, and Suess, Phys. Rev. **75**, 1766 (1949).
[14] M. G. Mayer, Phys. Rev. **75**, 1969 (1949).

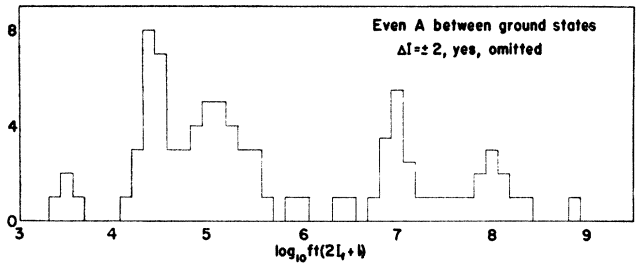

FIG. 11. Histogram of ft values for transitions between ground states of even nuclei. Transitions involving a spin change of two units and a parity change are omitted.

momentum operators respectively of the nucleons.[12] The selection rule $\Delta I=0$(yes) is obvious in the non-relativistic approximation (since $\boldsymbol{\sigma}\cdot\mathbf{p}$ is a pseudoscalar in three space), but also holds rigorously. Sufficient conditions to make the matrix elements of γ_5 vanish for even A are (a′) identical with a above, (b′) the ground states of odd-odd nuclei have $I>0$ (at least when the parity is odd). The desired conclusion now follows from the selection rule. In this case the "missing" group is compatable with all the current versions of the shell model.

Knowledge of the spins involved in the transitions singled out by the criteria A odd and $\log ft\sim 6.2$ would permit distinguishing between the two theoretical interpretations; the finding of many examples with $\Delta I=\pm 1$ would demonstrate the importance of tensor coupling while $\Delta I=0$ only would strongly favor axial vector coupling. Considering the possible overlapping of ft values for allowed and first forbidden transitions the occurrence of a few examples with $\Delta I=\pm 1$ would not exclude the second possibility.†

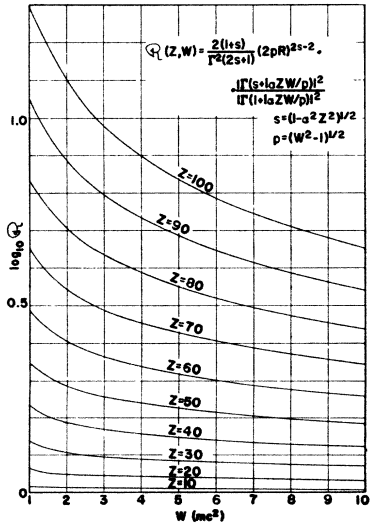

FIG. 12. The function $\mathfrak{R}(Z, W)$ used in the approximations described in Appendix A.

† *Note added in proof:* the α matrix elements also occur in the polar vector covariant formulation of the theory. This possibility in conjunction with axial vector coupling would permit both $\Delta I=\pm 1$ and $\Delta I=0$.

We are indebted to Professor K. Lark-Horovitz, Dr. D. J. Tendam, Professor C. S. Cook and Mr. G. E. Owen for information on decay schemes (particularly In^{112} and Cu^{61} and to Professor A. C. G. Mitchell for a prepublication copy of his excellent review of nuclear spectroscopy. We also wish to thank Drs. M. E. Rose and N. Tralli for information relating to the effect of the non-coulombian field within the nucleus on the electron wave functions and on the energy spectrum. Fortunately the effect on the energy spectrum is small.

APPENDIX A. EVALUATION OF $f_\pm$ AND f_k

Notation

Z-atomic number of product nucleus, positive for negatron emission, negative for positron emission.

$$p=(W^2-1)^{\frac{1}{2}},\quad s=(1-\alpha^2Z^2)^{\frac{1}{2}},\quad \alpha\sim 1/137$$

$$x=1-s,\quad y=\alpha ZW/p,\quad R\sim\tfrac{1}{2}\alpha A^{\frac{1}{3}}\text{ in units of }\hbar/mc.$$

$$F(Z,W)=\frac{2(1+s)}{(2s)\,!^2}(2pR)^{-2x}e^{\pi y}|\,(-x+iy)\,!\,|^2$$
$$=\mathfrak{R}(x,y)F_0(y)\qquad\text{(A1)}$$

$$F_0(y)=2\pi y/(1-e^{-2\pi y})$$

$$\mathfrak{R}(x,y)=\frac{2(1+s)}{(2s)\,!^2}(2pR)^{-2x}\left|\frac{(-x+iy)\,!}{(iy)\,!}\right|^2\qquad\text{(A2)}$$

$$f_\pm=f(Z,W_0)=\int_1^{W_0}F(Z,W)pW(W-W_0)^2dW$$
$$=\langle\mathfrak{R}(x,y)\rangle f^0(Z,W)$$
$$f^0(Z,W)=\int_1^{W_0}F_0(y)pW(W-W_0)^2dW.\qquad\text{(A3)}$$

The function $\ln|\,(-x+iy)\,!/(iy)\,!\,|^2$ can be expressed as a rapidly converging power series in x with coefficients given by easily computed functions of y^2 (note that $\mathfrak{R}$ is an even function of Z). Figure 12 exhibits $\mathfrak{R}(x, y)$ as a function of W and Z. In many applications the factor $\mathfrak{R}$ may be replaced by an average value $\langle\mathfrak{R}(x, y)\rangle$ and the average approximated by $\mathfrak{R}(x, \bar{y})$ evaluating $\bar{y}$ at a mean energy, most simply at $\bar{W}\sim\frac{1}{2}\cdot(W_0+1/W_0)$. The usual[1,15] analytical expression for $f_\pm$ involves even cruder approximations.

Two distinct expansion procedures are useful in evaluating f^0. The first, valid for small Z, is derived from the formal representation of $F_0(y)$ as a power series in $2\pi y$:

$$F_0(y)=1+\tfrac{1}{2}\cdot(2\pi y)+1/12\cdot(2\pi y)^2$$
$$-1/720\cdot(2\pi y)^4+\cdots.\qquad\text{(A4)}$$

What is notable in Eq. (A4) is the absence of a third power term and the small coefficient of the fourth power

[15] L. W. Nordheim and F. L. Yost, Phys. Rev. **51**, 942 (1937).

term. We find by numerical trial that the quadratic polynomial represents $F_0(y)$ with better than 90 percent accuracy on the range $-2\leqq 2\pi y\leqq 3$. The inequality

$$1-1/W_0^2>\left(\frac{Z}{40}\right)^2 \tag{A5}$$

defines the range on which the substitution of the quadratic polynomial for $F_0(y)$ introduces less than 10 percent error in the evaluation of f^0. On this range

$$f^0\cong f_{0a}+\pi\alpha Z f_{0b}+\tfrac{1}{3}\cdot(\pi\alpha Z)^2 f_{0c}$$

$$f_{0a}=\int_1^{W_0} pW(W-W_0)^2dW$$

$$=(W_0^2-1)^{\frac{1}{2}}[1/30\cdot W_0^4-3/20\cdot W_0^2-2/15]+\frac{W_0}{4}\ln(W_0+(W_0^2-1)^{\frac{1}{2}})$$

$$f_{0b}=\int_1^{W_0} W^2(W-W_0)^2dW$$

$$=1/30\cdot(W_0-1)^3(W_0^2+3W_0+6)$$

$$f_{0c}=\int_1^{W_0}\frac{1}{p}W^3(W-W_0)^2dW$$

$$=(W_0^2-1)^{\frac{1}{2}}\left[1/30\cdot W_0^4+\frac{11}{60}W_0^2+8/15\right]-\tfrac{3}{4}\cdot W_0\ln(W_0+(W_0^2-1)^{\frac{1}{2}}). \tag{A6}$$

For small values of W_0-1

$$f_{0a}=\frac{16\times 2^{\frac{1}{2}}}{105}(W_0-1)^{7/2}\times\left[1+\frac{5}{12}(W_0-1)+\frac{35}{1056}(W_0-1)^2+\cdots\right]$$

$$f_{0c}=\frac{8\times 2^{\frac{1}{2}}}{15}(W_0-1)^{5/2}\times\left[1+\frac{11}{28}(W_0-1)+\frac{25}{224}(W_0-1)^2+\cdots\right]. \tag{A7}$$

The application of Eqs. (A6) and (A7) to H^3 is particularly instructive. Here $W_0-1=0.036$, $\pi\alpha Z=0.0459$ and $f_-\cong f^0(2, W_0)\cong(1.96+0.72+0.128)10^{-6}=2.81\times 10^{-6}$ checking an earlier evaluation by the method of numerical integration.[16]

An explicit formula for $\bar{W}-1$, based on the quadratic polynomial approximation to $F_0(y)$ is developed in Appendix *B*.

[16] E. J. Konopinski (private communication).

Equations (A2) and (A3) yield a useful relation between $f^0(Z, W_0)$ and $f^0(-Z, W_0)$. From Eq. (A2)

$$F_0(y)=2\pi y\left[1+\frac{e^{-2\pi y}}{1-e^{-2\pi y}}\right]=2\pi y+F_0(-y). \tag{A8}$$

Consequently

$$f^0(-Z, W)=-2\pi\alpha Z\int_1^{W_0} W^2(W_0-W)^2dW+f^0(Z, W). \tag{A9}$$

A second expansion procedure, valid for sufficiently large values of Z and W, is based on the identity

$$1-e^{-2\pi y}=(1-e^{-2\pi\alpha Z})\left[1+\frac{1-e^{-2\pi(y-\alpha Z)}}{e^{2\pi\alpha Z}-1}\right], \tag{A10}$$

and the assumed inequality

$$\frac{1-e^{-2\pi(y-\alpha Z)}}{e^{2\pi\alpha Z}-1}<1. \tag{A11}$$

In view of Eq. (A9) only positive values of Z (negatron emission) need be considered in the mathematical development. Equations (A10) and (A11) then permit the expansion

$$F_0(y)=\frac{2\pi y}{1-e^{-2\pi\alpha Z}}\left[1-\frac{1-e^{-2\pi(y-\alpha Z)}}{e^{2\pi\alpha Z}-1}+\left\{\frac{1-e^{-2\pi(y-\alpha Z)}}{e^{2\pi\alpha Z}-1}\right\}^2+\cdots\right]. \tag{A12}$$

The convergence condition of Eq. (A11) is equivalent to

$$e^{-2\pi y}+1>2e^{-2\pi\alpha Z}. \tag{A13}$$

For $2\pi\alpha Z\ll 1$, Eq. (A13) holds provided only that $W>2/(3^{\frac{1}{2}})=1.155$. The inequality holds for all values of W/p if $\exp(2\pi\alpha Z)>2$ or $Z>15$. In the next step $2\pi(y-\alpha Z)$ is treated as a small quantity and $W/p-1$ replaced by the leading terms in the expansion in powers

TABLE AI. Coefficients in Eq. (A14).

Z	$2\pi\alpha Z$	$U_1(Z)$	$U_1(-Z)$	$U_2(Z)$	$U_3(Z)$
0	0	1.000	1.000	−1.000	−1.000
10	0.458	1.246	0.799	−0.981	−0.927
20	0.917	1.528	0.611	−0.933	−0.803
30	1.375	1.840	0.465	−0.856	−0.595
40	1.834	2.183	0.349	−0.762	−0.357
50	2.292	2.550	0.258	−0.657	−0.126
60	2.751	2.936	0.188	−0.551	0.070
70	3.209	3.344	0.135	−0.452	0.217
80	3.668	3.763	0.096	−0.361	0.310
90	4.126	4.194	0.0675	−0.283	0.354
100	4.585	4.631	0.0472	−0.217	0.364

of $1/W^2$. In this way Eq. (A12) is reduced to

$$\frac{p}{W}F_0(y)\cong U_1(Z)+U_2(Z)/2W^2+U_3(Z)/8W^4 \quad \text{(A14)}$$

with

$$U_1(Z)=\frac{2\pi\alpha Z}{1-e^{-2\pi\alpha Z}}$$

$$U_2(Z)=-U_1^2(Z)e^{-2\pi\alpha Z}$$

$$U_3(Z)=-U_2(Z)[2\pi\alpha Z-3+2U_1(-Z)]. \quad \text{(A15)}$$

For positron emission the only change is the replacement of $U_1(Z)$ in Eq. (A14) by

$$-2\pi\alpha Z+U_1(Z)=U_1(-Z). \quad \text{(A16)}$$

The other coefficients $U_2(Z)$ and $U_3(Z)$ are even functions of Z. Numerical values of U_1, U_2 and U_3 are listed in Table AI. The accuracy of Eq. (A14) has been tested by numerical calculations. At $Z=20$ the error in the approximate formula is less than 4 percent for all values of W and still smaller for larger values of Z.

Equation (A14) yields

$$f^0\cong U_1f_{01}+U_2f_{02}+U_3f_{03}$$

$$f_{01}=\int_1^{W_0}W^2(W-W_0)^2dW$$

$$=1/30\cdot(W_0-1)^3(W_0^2+3W_0+6)$$

$$f_{02}=\tfrac{1}{2}\cdot\int_1^{W_0}(W-W_0)^2dW=\tfrac{1}{6}\cdot(W_0-1)^3$$

$$f_{03}=\tfrac{1}{8}\cdot\int_1^{W_0}(W_0-W/W)^2dW$$

$$=\tfrac{1}{8}\cdot[W_0^2-1-2W_0\ln W_0]. \quad \text{(A17)}$$

For $Z\geqq 20$, Eq. (A17) is entirely adequate without restriction on W_0. The error is everywhere less than 4 percent and for large values of Z even less than 1 percent. Furthermore the error is still small without restriction on Z (positive or negative) if $W_0>2$.

The uncertainty in the evaluation of $\langle\Re(x,y)\rangle$ by the crude procedure described earlier introduces an error of unknown magnitude in the evaluation of $f(Z,W_0)$ by means of Eqs. (A3) and (A17). To control this error and to extend the accurate evaluation into regions not covered by the approximate formulas, a number of points on the charts were computed by numerical integration of the definite integral defining $f(Z,W_0)$. For this purpose accurate tables of the Fermi function were required. A table prepared by the Bureau of Standards was found useful. Additional values were computed with the aid of Stirling's asymptotic formula for the gamma-function of large argument. The more convenient procedure based on Fig. 10 was not available until most of the calculations had been completed.

It was found possible to maintain an accuracy of better than 90 percent in $f(Z,W_0)$ over the entire range of Z and W_0. On the logarithmic plots the errors in $\log_{10}f(Z,W_0)$ are less than 0.04 in absolute magnitude.

All values of f_k appearing in the charts are computed from the allowed formula

$$f_k=2\pi(\alpha Z)^{2s+1}(2R)^{2s-2}\frac{(1+s)}{\Gamma(2s+1)}(W_0+s)^2. \quad \text{(A18)}$$

The values of f_+ and f_- used in preparing the charts were calculated by numerical integration for $W_0<5$. For $W_0\geqq 5$, the Nordheim and Yost approximation was used, with one modification: it was found to require multiplication by the factor $[(1+C(\alpha Z)^2)/(1+(\alpha Z)^2)]$, where C is Euler's constant $0.577\cdots$, to allow for the presence of an exponential factor in the approximate formula for the gamma-function which was neglected by Nordheim and Yost. With this modification, the two methods agree satisfactorily at the point $W_0=5$, where both were used; check points indicate that the agreement extends to all larger values of W_0, and to lower values for certain ranges of Z.

APPENDIX B. AVERAGE ENERGY

For small Z and $W_0-1\ll 1$ the average energy is given by the formula

$$\bar{W}=1+\frac{\eta_a+(\pi\alpha Z)\eta_b+\frac{1}{3}\cdot(\pi\alpha Z)^2\eta_c}{f_{0a}+(\pi\alpha Z)f_{0b}+\frac{1}{3}\cdot(\pi\alpha Z)^2f_{0c}} \quad \text{(B1)}$$

in which

$$\eta_a=\int_1^{W_0}W(W-1)(W-W_0)^2dW$$

$$\eta_b=\int_1^{W_0}W^2(W-1)(W-W_0)^2dW$$

$$\eta_c=\int_1^{W_0}\frac{W^3}{p}(W-1)(W-W_0)^2dW. \quad \text{(B2)}$$

The evaluation of Eqs. (B2) as power series in $\eta=W_0-1$ yields

$$\eta_a=\frac{16\times 2^{\frac{1}{2}}}{315}\eta^{9/2}\left[1+\frac{25}{44}\eta+\frac{245}{32\times 143}\eta^2+\cdots\right]$$

$$\eta_b=\frac{1}{12}\eta^4\left[1+\frac{4}{5}\eta+\frac{1}{5}\eta^2\right]$$

$$\eta_c=\frac{8\times 2^{\frac{1}{2}}}{105}\eta^{7/2}\left[1+\frac{11}{12}\eta+\frac{125}{352}\eta^2+\cdots\right]. \quad \text{(B3)}$$

A tedious algebraic reduction employing a new variable $q=\pi\alpha Z/\eta^{\frac{1}{2}}$ yields the convenient form

$$3\frac{\bar{W}-1}{W_0-1}=(1+0.1515\eta-0.0427\eta^2)\cdot\frac{1+1.160q(1+0.2320\eta+0.0166\eta^2)+0.5q^2(1+0.3480\eta+0.1032\eta^2)}{1+1.547q(1+0.0825\eta-0.0322\eta^2)+1.167q^2(1-0.0238\eta+0.0884\eta^2)}. \quad \text{(B4)}$$

In the application to H^3, $\eta\sim0.0365$, $q\sim0.242$ and

$$\begin{aligned}\bar{W}-1&=0.3053(W_0-1)\\&=0.3053\times18.6\text{ kv}\\&=5.68\text{ kv}.\end{aligned} \quad \text{(B5)}$$

checking an earlier evaluation by the method of numerical integration[17] and checking also the independent experimental determinations of $\bar{W}$ and W_0 as discussed in reference 17.

[17] Slack, Owen, and Primakoff, Phys. Rev. **75**, 1448 (1949).

Erratum: Theory of the Origin and Relative Abundance Distribution of the Elements

[Rev. Mod. Phys. **22**, 153 (1950)]

RALPH A. ALPHER AND ROBERT C. HERMAN
Applied Physics Laboratory, The Johns Hopkins University, Silver Spring, Maryland

ON p. 204 the graphs in Figs. 23 and 24 should be interchanged, leaving the legends and figure numbers unchanged.